Quantifying Aflatoxin B1 in peanut oil using fabricating fluorescence probes based on upconversion nanoparticles.

Quantifying Aflatoxin B_1 in peanut oil using fabricating fluorescence probes based on upconversion nanoparticles

Cuicui Sun, Huanhuan Li, Anastasios Koidis, Quansheng Chen*

School of Food and Biological engineering, Jiangsu University, Zhenjiang, 212013, P. R. China.

Institute for Global Food Security, Queen's University Belfast, BT95GN, Northern Ireland, United Kingdom.

* Corresponding author. Tel.: +86-511-88790318; fax: +86-511-88780201

E-mail: qschen@ujs.edu.cn (Qs Chen)

ABSTRACT

Rare earth doped upconversion nanoparticles convert near-infrared excitation light into visible emission light. Compared to organic fluorophores and semiconducting nanoparticles, upconversion nanoparticles (UCNPs) offer high photochemical stability, sharp emission bandwidths, and large anti-Stokes shifts. Along with the significant light penetration depth and the absence of autofluorescence in biological samples under infrared excitation, these UCNPs have attracted more and more attention on toxin detection and biological labelling. Herein, the fluorescence probe based on UCNPs was developed for quantifying Aflatoxin B_1 (AFB_1) in peanut oil. Based on a specific immunity format, the detection limit for AFB_1 under optimal conditions was obtained as low as 0.2 $ng \cdot mL^{-1}$, and in the effective detection range 0.2 to 100 $ng \cdot mL^{-1}$, good relationship between fluorescence intensity and AFB_1 concentration was achieved under the linear ratios up to 0.90. Moreover, to check the feasibility of these probes on AFB_1 measurements in peanut oil, recovery tests have been carried out.A good accuracy rating (%) was obtained in this study. results showed that the nanoparticles can be successfully applied for sensing AFB_1 in daily edible oils.

Keywords: rapid toxin detection; biological labelling; upconversion nanoparticles; Fluorescence probes

1. Introduction

China and India regions is the world's biggest market for peanut and its derivatives (in particular peanut oil) in terms of productions well as consumption (Sanders Iii et al., 2014). Several survey studies have shown that mold will grow quickly, and the possible presence of aflatoxins would transfer into peanut oil, when peanuts are stored for weeks in humid conditions (Klu & Chen, 2015). Aflatoxins are a group of highly toxic secondary metabolites produced mainly by Aspergillus *flavus* and Aspergillus *parasiticus* on a variety of food products (~~K.~~ Chen et al., 2014). These toxins are known to be potent carcinogens, teratogens, mutagens, and immunosuppression and pose harmful threat to animal and human health (Xia et al., 2013). Naturally occurring aflatoxins are composed of B_1, B_2, G_1 and G_2 types. Among them, aflatoxin B_1 (AFB_1) is the most abundant and carcinogenic (Passone, Girardi, & Etcheverry, 2013). Since peanut oil is widely consumed as diet in the Asian region, even low levels of contamination may cause severe health and safety incidents (Luongo et al., 2013; Quiles, Manyes, Luciano, Mañes, & Meca, 2015; Van de Perre, Jacxsens, Lachat, El Tahan, & De Meulenaer, 2015). Therefore, determination of AFB_1 in peanut and its derivatives becomes a subject of great importance for industries and regulators alike.

A wide range of methods are currently available, including thin layer chromatography (TLC), spectrometry (Busman, Liu, Zhong, Bobell, & Maragos, 2014), gas chromatography(Ceker, Agar, Alpsoy, Nardemir, & Kizil, 2014), High-performance liquid chromatography (HPLC)(Herzallah, 2009), fluorescence polarization assays(Maragos, 2009), radio immunoassays(Waliyar, Reddy, & Lava-Kumar, 2009), enzyme-linked immunosorbent assay(Sai et al., 2010) (ELISA) and fiberoptic based immunoassays(Kozlov et al., 2004), which have been used for the detection of aflatoxins. However, most of these techniques require well equipped laboratories, trained personnel, harmful

48 solvents, and are time-consuming. Therefore, the demand for developing a rapid and sensitive
49 method for sensing aflatoxins is urgent.

50 In optical detection methods, conventional downconversion fluorescent materials, such as
51 semiconductor nanoparticles, dye-coupled hybrid materials and mesoporous silica, are fluorophores
52 that are commonly used in biological studies and clinical application because of their unique features
53 (Mnoyan, Kirakosyan, Kim, Jang, &Jeon, 2015); Sharma, Rawat, Solanki, & Bohidar, 2015). One
54 important intrinsic limitation, however, is that these materials usually emit one lower-energy photon
55 after absorption of a higher-energy ultraviolet or visible photon. This lead to significant
56 disadvantages, such as low light-penetration depth, potentially severe photodamage to living
57 organisms (Sozer & Kokini, 2014), and the autofluorescence (noise) of some biological samples. To
58 solve these problems, the development of alternative biological luminescent labels through the use of
59 up-converting rare-earth nanophosphors (UCNPs) has attracted a tremendous amount of attention
60 due to the unique luminescence properties of rare-earth nanoparticles. Lanthanide-doped,
61 near-infrared (NIR)-to-visible upconversion nanophosphors are capable of emitting strong visible
62 fluorescence under the excitation of NIR light (typically 980 nm). They have been shown to have
63 significant advantages as fluorescent bio-label (Boyer, Manseau, Murray, & van Veggel, 2010;
64 Chatterjee, Rufaihah, & Zhang, 2008; Fang et al., 2014; Huang, Yu, & Chu, 2015; Ma, Liu, Han,
65 Yang, & Liu, 2015; Tian et al., 2015) over the traditional organic fluorophores due to their attractive
66 optical and chemical features, including low toxicity (Chatterjee, Gnanasammandhan, & Zhang,
67 2010; Zhang, Wu, Tang, Su, & Lv, 2014), large stokes shifts (Ahn et al., 2016), high resistance to
68 photobleaching(Feng Wang et al., 2011), blinking, photochemical stability (H. Q. Chen, Yuan, &
69 Wang, 2013) and the lack of both auto-fluorescence (Aramburu et al., 2015) and light scattering

background (Zhou, Liu, & Li, 2012). As a result, the signal-to-background ratio and sensitivity of the detection can be greatly improved. Moreover, upconversion nanoparticles have also attracted increasing interest due to their optical properties which can be achieved by adding a $\lambda_{exc.}$ = 980 nm optical source used in fluorescence measurement. From the mentioned advantages above, we can conclude that the upconversion nanophosphors as color label has a high potential on the detection of toxin.

In recent years, with the rapid development of nanostructured materials and nanotechnology in the fields of biotechnology and contaminat detection, magnetic nanoparticles (MNPs) have been receiving considerable attention. Due to their magnetic properties, low toxicity, and biocompatibility, MNPs are useful for the separation of target antibiotics from a mixture of antibiotics and matrix substances. Additionally, MNPs help to concentrate the separated antibiotics into a small volume, which is suitable for impedance measurements(Z. Wang et al., 2013). Artificial antigen-modified MNPs were employed as immune sensing probes, and antibody functionalized UCNPs were used as signal probes; the antibodies-functionalized UCNPs were linked to the surface of the MNPs by antibody–antigen affinity.

Herein, we explored a novel and sensitive fluorescence probe for sensing toxin by crosslinking rare earth doped upconversion nanoparticles and immunoproteins. Fig. 1 presents the scheme of this proposed fluorescence bioassay platform. Specific procedures are outlined as follows. (1) Upconversion nanoparticles (UCNPs) were synthesized and functionalized. (2) The resultant water-soluble UCNPs were conjugated with anti-AFB_1 antibodies to produce biological fluorescent probes. (3) A fluorescence standard curve was prepared with different concentrations of AFB_1. (4) Independent food samples were tested. As an efficient, specific, and technically simple biological

probe, these selective sensors can be used for rapidly detecting toxin in food.

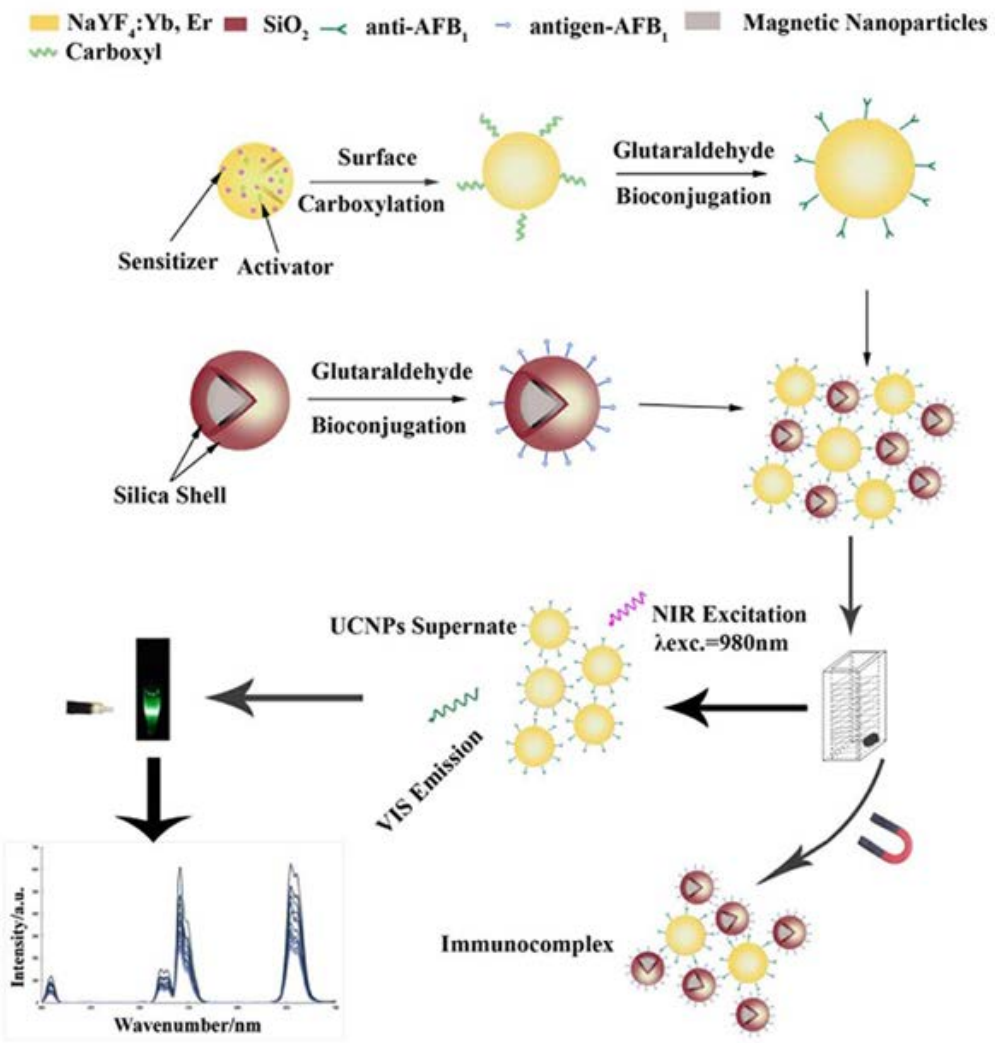

Fig. 1. Scheme of this proposed fluorescence bioassay platform.

2. Materials and methods

2.1 Instruments

The size and morphology of nanoparticles were determined using a JEM-2100HR transmission electron microscope (TEM, JEOL Ltd., Japan). X-ray diffraction (XRD) measurements were performed using a D8-advance instrument (Bruker AXS Ltd., Germany). Upconversion fluorescence

spectra were measured using an F-7200 fluorescence spectrophotometer (Hitachi Co., U.S.A.) modified with an external 980nm laser (Beijing Hi-Tech Optoelectronic Co., China) instead of the internal excitation source. Fourier transform infrared spectrophotometer (FT-IR) spectra of the nanoparticles were obtained with a Nicolet Nexus 470 (Thermo Electron Co., U.S.A.) using a KBr detector.

2.2 Reagents

AFB_1 standard solution, (8 $mg \cdot mL^{-1}$ solution in methanol and working dilution by deionized water),AFB_1–BSA antigen (extent of labeling 8-12 mol Aflatoxin B_1 per mol BSA), monoclonal anti-AFB_1 antibody, (6 $mg \cdot mL^{-1}$ solution and working dilution by phosphate buffer solution) was obtained from Beijing Mozhidong Bio-tech (city. Country). Hydrated rare earth nitrate ($RECl_3 \cdot xH_2O$, RE Y, Yb, Er, ≥ 99.99%), oleic acid (≥ 90%) and octadecanoic acid (≥ 90%) were purchased from Sigma-Aldrich (Shanghai, China). In addition, $FeCl_3 \cdot 6H_2O$, sodium fluoride, sodium hydroxide, methyl alcohol, toluene, ethyl alcohol, sodium citrate, 1,6-hexanediamine, anhydrous sodium acetate, glycol, bovine serum albumin (BSA, 96-99%),25% glutaraldehyde, tetraethyl orthosilicate (TEOS ≥ 98%), and 3-aminopropyltrimethoxysilane (APTES) was all purchased from Sinopharm Chemical Reagent Co., Ltd. (Shanghai, China). All the chemicals used were of analytical grade. The water used was deionized.

2.3 Synthesis and surface modification of rare-earth-doped

Oleic acid-capped $NaYF_4$: Yb, Er UCNPs were synthesized according to the method reported in predecessors' research (F. Wang et al., 2010) with a few modifications. In a typical experiment, 2 ml of $RECl_3$ (0.2 M, RE = Y (78%), Yb (20%), Er (2%)) in methanol were added to a 50 ml flask containing 3 ml oleic acid and 7 ml 1-octadecene, and the solution was heated to 160 ℃ for 30 min

and then cooled down to room temperature. Thereafter, 5 ml methanol solution of NH_4F (1.6 mmol) and NaOH (1 mmol) was added and the solution was stirred for 30 min. After methanol evaporated, the solution was heated to 300 ℃ under argon for 1.5 h and cooled down to room temperature. The resulting nanoparticles were precipitated by the addition of ethanol, collected by centrifugation, washed with methanol and ethanol several times, and finally dried in an oven at 60 ℃.

The obtained oleic acid-capped UCNPs can disperse well in nonpolar solvents. However, for biological applications, hydrophobic UCNPs should be converted into hydrophilic UCNPs so as to be compatible with biomolecules, such as antibodies. Thus, surface modification of the hydrophobic UCNPs was performed via a ligand exchange process as described in predecessors' research (Ong, Ang, Alonso, & Zhang, 2014). Briefly, a mixture of 2 mmol sodium citrate in 15 ml of diethylene glycol was first heated to 110 ℃ under argon for 30 min. Oleic acid-capped UCNPs (10 mg) dispersed in cyclohexane and toluene were then added into the mixture and the reaction was heated to 160 ℃ for evaporation of cyclohexane and toluene. After complete evaporation, the reaction was further maintained at 160 ℃ for 3 h. Water-soluble UCNPs were then collected by centrifugation, washed with ethanol and ultrapure water several times, and finally dispersed in ultrapure water.

2.4 Preparation of amine-functionalized Fe_3O_4 magnetic nanoparticles

Amine-functionalized Fe_3O_4 MNPs were prepared according to Gao's work (Gao, Gu, & Xu, 2009). Briefly, a solution of 6.5 g 1,6-hexanediamine, 2.0 g anhydrous sodium acetate and 1.0 g $FeCl_3$ $6H_2O$ as a ferric source in 30 mL glycol was stirred vigorously at 50 ℃ to give a transparent solution. This solution was then transferred into a Teflon-lined autoclave and reacted at 198 ℃ for 6 h. The MNPs were then rinsed with water and ethanol (2 or 3 times) to effectively remove the

147 solvent and unbound 1,6-hexanediamine, and then dried at 50 ℃ before characterization and
148 application. During each rinsing step, the nanoparticles were separated from the supernatant by using
149 magnetic force.

150 *2.5 Preparation of immunosensing probes and signal probes*

151 The artificial antigen conjugated MNPs and antibody conjugated immunosensing probes were
152 fabricated with the classical glutaraldehyde method. Typically, 10 mg of MNPs were dispersed in 5
153 mL of 10 mmol/L phosphate buffer solution (pH 7.4) by ultrasonication for 20 min. 1.25 mL of 25%
154 glutaraldehyde was then added to the mixture. The mixture was shaken slowly at room temperature
155 for 1 h, and the Fe_3O_4 MNPs were separated by an external magnetic field and washed with PBS
156 three times to remove the physically adsorbed glutaraldehyde. Subsequently, 11.67 μL of AFB_1-BSA
157 antigen, at a concentration of 6 mg mL^{-1}, was added into 5 mL of a suspension of Fe_3O_4 MNPs in
158 PBS. The mixture was shaken slowly for 6 h at room temperature. The surplus biomolecules were
159 removed by magnetic separation of the particles from the solution. The AFB_1–BSA antigen
160 conjugated MNPs were treated with 5 mL BSA at 3% concentration in 10 mmol/L PBS at room
161 temperature for 6 h to block the unreacted and nonspecific sites. Finally, the as-prepared probes were
162 stored in 5 mL of 10 mmol/L PBS at 4 ℃ prior to use. The biofunctionalization of amino-modified,
163 water-soluble UCNPs conjugated with monoclonal antibody, namely the preparation of the signal
164 probes, was similar to that of the antigen conjugated MNPs described above. The prepared antigen
165 conjugated Fe_3O_4 MNPs and antibody functionalized UCNPs were characterized by FT-IR
166 spectroscopy.

167 *2.6 Sample preparation and measurement*

168 Twelve naturally contaminated peanut oil samples obtained from local supermarkets were

169 treated according to official methods of China (*GB/T, 2003*) with some modifications. Briefly, five
170 grams of each peanut oil sample and 5 g NaCl were introduced into a 100 mL flask, and the
171 extracting solution (methanol:water; 7:3 (v:v)) was filled to the mark, completely mixed with the
172 compound and then the mixture was transferred into the cup of a homogenizer. The mixture was then
173 stirred at high-speed and extracted for 2 min. Next, the resulting solution was filtered, and 10 mL of
174 filtrate was transferred into a 50 mL flask; water was filled to the mark, and the flask contents were
175 mixed to homogeneity. The resulting mixture was further filtered with glass fiber filter paper until
176 the filtrate was clear. For the standard addition and recovery experiments, the AFB_1 standard
177 solutions were added to the peanut oil samples before adding the extracting solution. After the
178 complete chemical reaction and magnetism separation, fluorescence spectra of the obtained
179 supernatants (from 400 to 700 nm) were measured with a fluorescence spectrophotometer equipped
180 with a 980 nm laser excitation under the excitation power (1.3 W). Here, the 541nm peak intensity
181 emission wavelength was used.

182 **3. Results and Discussion**

183 *3.1 Characterization of the prepared upconversion nanoparticles and magnetic nanoparticles*

184 Results showed that toxin-specific antibodies with high selectivity and sensitivity were
185 successfully conjugated onto the surface of UCNPs to yield UCNP−antibody probes, as illustrated in
186 Fig.1. Prior to the conjugation, the precursor UCNPs were first characterized by transmission
187 electron microscopy (TEM), X-ray diffraction (XRD) and fluorescence spectral measurements, as
188 shown in Fig 2. Successful surface modification, selectivities, sizes, and luminance and spectral
189 properties of UCNPs before and after surface modification were validated by TEM and fluorescence
190 spectral measurements, as presented in Fig.2 (a, b, c). The TEM images confirmed the hexagonal

UCNP structures and revealed that the particles were uniform with an average diameter of approximately 50 nm before and after surface modification and bioconjugation. The fluorescence spectra of the UCNPs showed the expected characteristic emission peaks at approximately 407, 542, and 657 nm upon NIR (980 nm) excitation, corresponding to blue, green, and red light, respectively (the naked-eye images in the inset show the visible intensity of the UCNPs). The peaks are ascribed to the transitions from the $^{2}H_{9/2}$, $^{4}S_{3/2}$, and $^{4}F_{9/2}$ levels to the $^{4}I_{15/2}$ ground state of the Er^{3+} ion (L. Wang, Li, & Li, 2007; Leyu Wang & Li, 2006). The fluorescence properties were also retained, as both the oleic acid-capped UCNPs and the water-soluble UCNPs showed the same characteristic emission peaks upon NIR excitation. Additionally, the diffraction peaks of the XRD pattern in Fig. 2 (d) were identified as pure hexagonal *β*-phase $NaYF_4$ crystals (JCPDS Standard Card *No. 16-0334*); no diffraction peaks corresponding to cubic phase crystals or other impurities were observed.

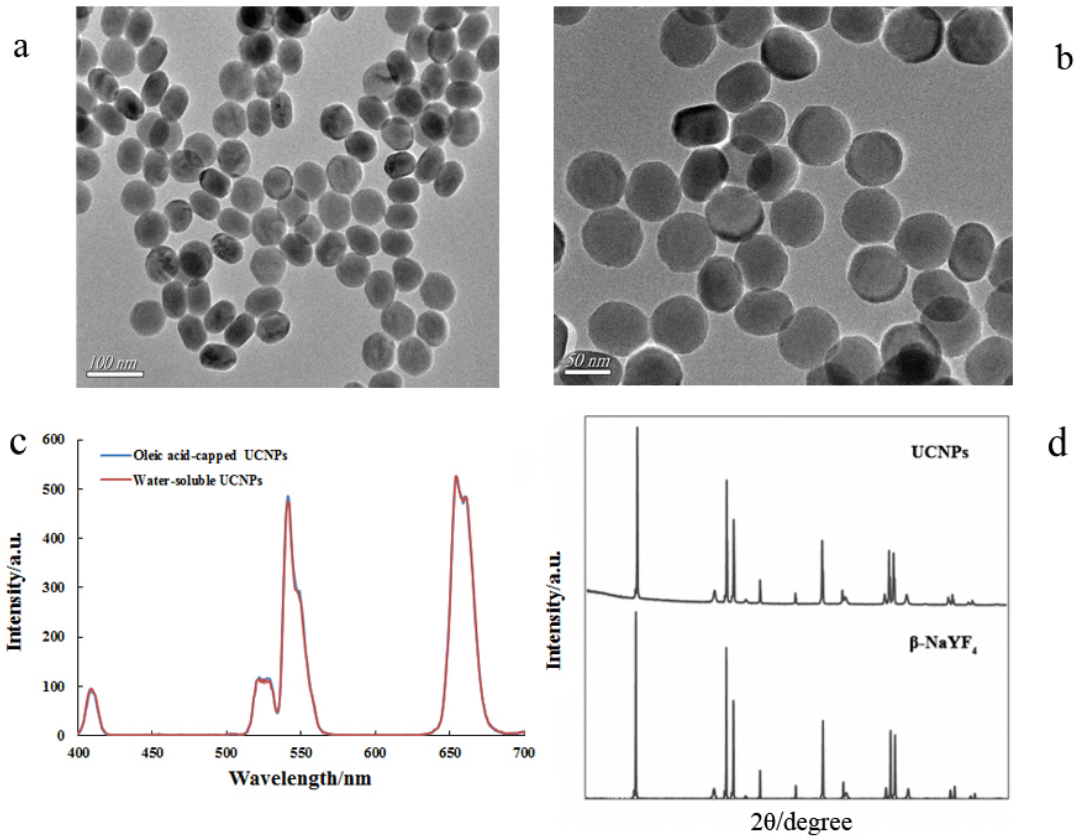

Fig. 2. TEM images of oleic acid-capped UCNPs (a) and water-soluble UCNPs (b), Fluorescence properties of

oleic acid-capped UCNPs and water-soluble UCNPs (c), XRD pattern of oleic acid-capped UCNPs (d).

The UCNPs used in this work were Yb, Er ion-pair doped hexagonal phase $NaYF_4$ nanoparticles. The hexagonal phase $NaYF_4$ was reported to be one of the most efficient hosts for performing infrared to visible photon conversion when activated by Yb, Er ion-pairs. During the experiment, we found that the reaction time and temperature were the two main influential factors in the phase transition of $NaYF_4$ UCNPs. In order to obtain hexagonal phase $NaYF_4$, the reaction was maintained at 300 ℃ for 1.5 h.

The XRD pattern of $NaYF_4$: Yb, Er phosphor gives several reflections shown in Fig.2 (d) indicates that the microballoon sphere are well-crystallized. In Yb^{3+} and Er^{3+} co-doped systems, Yb^{3+} ions act as sensitizers and Er^{3+} ions as activators. The Debye Scherrer formula was used to calculate the crystallite size of the synthesized phosphor and is given by $d = \frac{0.89\lambda}{\beta \cos\theta}$, where d is the crystallite size, λ is the wavelength of the X-rays, β is full width at half maximum and θ is the diffraction angle. The average value of the crystallite size was found to be around 50 nm that confirms the formation of nanostructured crystallites.

Fig. 3 (a, b) displays the TEM and selected area electron diffraction (SAED) images of amino-modified MNPs confirming good dispersibility and morphology with an average size of about 20 nm. In addition, the crystalline structure and phase purity was determined by powder XRD as shown in Fig. 3 (c). The positions and relative intensities of all diffraction peaks matched well with those from the JCPDS card (*No.52-0102*) for magnetite. The sharp, strong peaks confirmed the products were well crystallized.

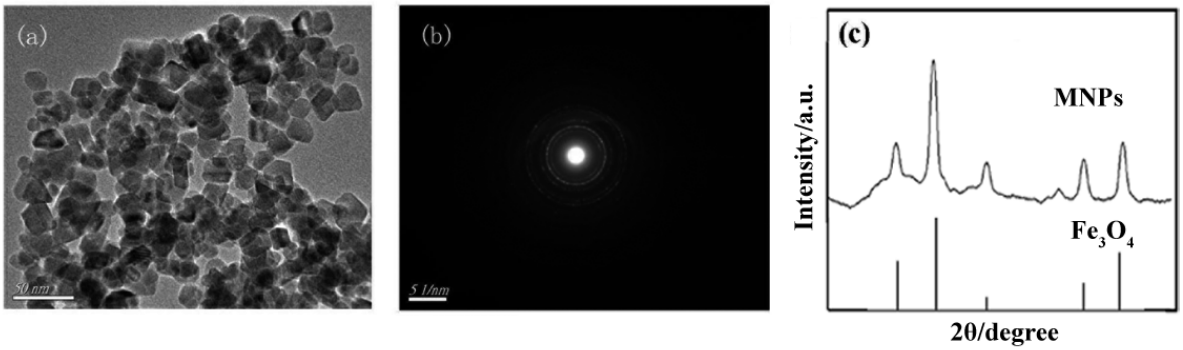

225

226 **Fig. 3**. TEM image (a), SAED image (b), and XRD (c) of the amino-functionalized magnetic nanoparticles.

227

228 *3.2 Characterization of the antigen modified MNPs and antibody functionalized UCNPs*

229 In this report, to verify the formation of the bionanoparticles, infrared spectroscopy was utilized
230 to monitor the reaction products in each derivatization step, and the results are shown in Fig. 4:
231 spectra of UCNPs (A), carboxylation-UCNPs (B), carboxylation-UCNPs−antibody probes (C),
232 amination-MNPs (D) and amination-MNPs-antigen. Fig. 4 (A, B, C, D and E) confirmed the
233 presence of carboxyl on the UCNPs, UCNP-antibody probes, UCNP-antibody-antigen-MNPs
234 compounds and antigen on the MNPs. More specifically, in Fig. 4 (A, B, C), the water-soluble
235 UCNPs presented with a single broad peak at 3427 cm^{-1}, corresponding to the stretching vibration of
236 hydroxide radicals (-OH). The characteristic peak at 1629 cm^{-1} is related to the asymmetric
237 stretching vibration of carboxyl groups (-COOH) of the citrate ligands on the surface of the UCNPs.
238 These two peaks indicated that the carboxyl groups from the ligand exchange were successfully
239 modified on the surface of UCNPs to produce water-soluble UCNPs. When the glutaraldehyde
240 crosslinking method -prepared antibodies were introduced, three characteristic peaks at 2360, 2335,
241 and 1396 cm^{-1} appeared. The peaks at 2360 and 2335 cm^{-1} corresponded to methylene stretching
242 vibrations ($-CH_2-$). The peak at 1396 cm^{-1} corresponded to carboxyl stretching vibrations (COO-)

due to the linking reaction between the water-soluble UCNPs and the antibodies. Furthermore, a new peak was observed at 1540 cm^{-1} upon comparison of the spectra of the UCNP-antibody-antigen-MNPs complex and the UCNP−antibody probe; this peak is attributed to the distinct amide I and amide II vibration modes characteristic of antigen proteins. On the other hand, in Fig. 4 (D, E), a new peak was observed at 1400 cm^{-1} upon comparison of the spectra of the amino-MNPs complex and the MNPs-antigen probes; this peak is attributed to the distinct amide I and amide II vibration modes characteristic of antigen proteins. In the FT-IR spectra of antigen-functionalized-Fe_3O_4 MNPs and antibody-functionalized-UCNPs, all the characterized peaks of Fe_3O_4 MNPs and UCNPs appeared in the corresponding wavenumbers, indicating the modification of antigen and antibody onto the surface of MNPs and UCNPs. On the basis of these characterizations, the proposed UCNP-based method is suitable for sensing toxin.

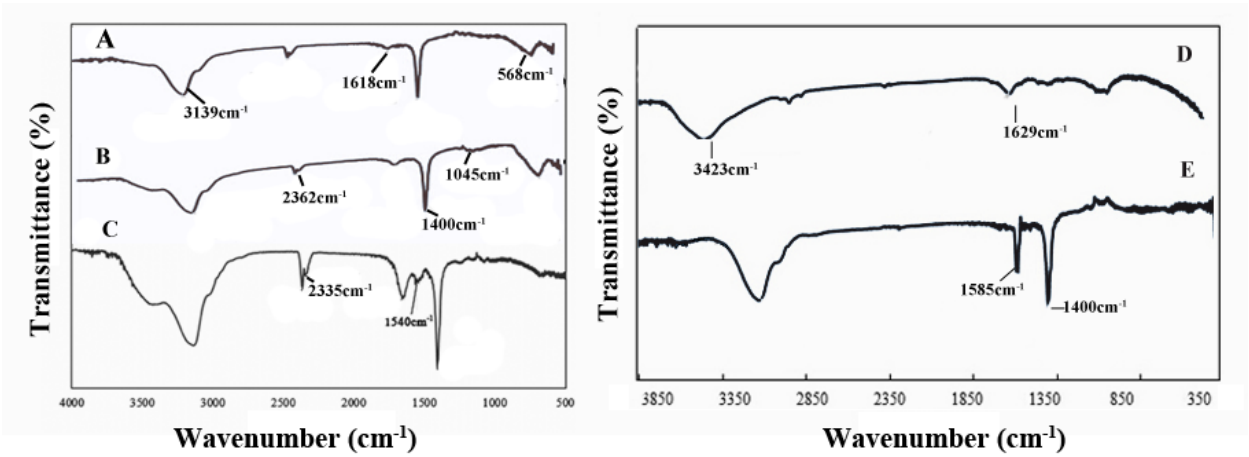

Fig.4. FT-IR spectrums of oleic acid-capped UCNPs (A), carboxylation-UCNPs (B), carboxylation-UCNPs−antibody probes (C), amination-MNPs (D) and amination-MNPs-antigen (E).

3.3 Specific Capturing Evaluation

In order to evaluate the specificity of the immunoassay procedure using this developed fluorescent probe for AFB_1, other two commonly occurring toxins, Aflatoxin G_1 (AFG_1) and

Fumonisin B_1 (FB_1) were examined, instead of AFB_1, with the developed fluorescent probe. Results were shown in Fig. 5, both AFG_1 and FB_1 caused negligible changes of the fluorescence, while a significant change of fluorescence was observed for AFB_1. Therefore, it is clearly demonstrated that the designed fluorescent probe has good specificity to capture AFB_1.

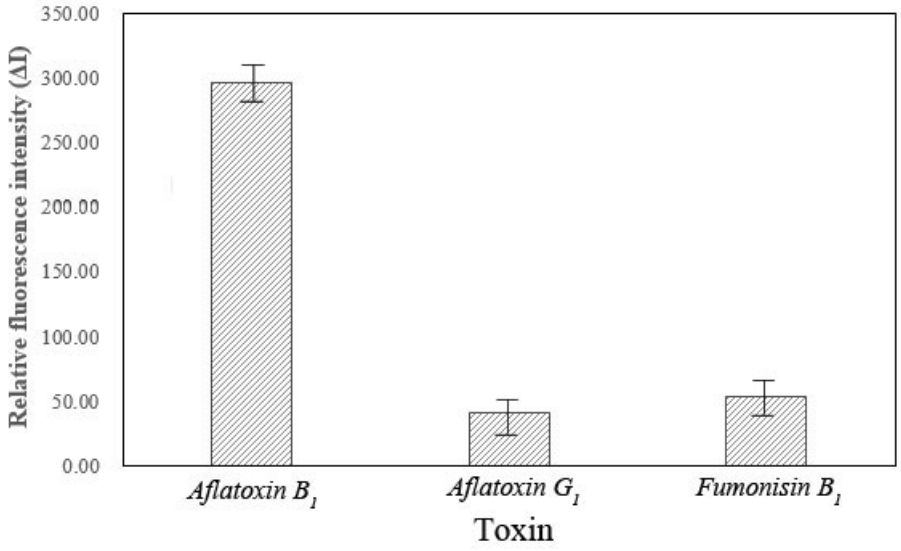

Fig. 5. Specific selectivity evaluation of the proposed method for AFB_1 (1 ng·ml^{-1}) against other toxin (1 ng·ml^{-1}).

3.4 Analytical performance

In a typical experiment, different concentrations of AFB_1 were incubated under agitation with the UCNP−antibody probes for 2 h at 37 ℃. On the basis of the specificity of the antibody for the AFB_1, UCNPs-antibody-antigen-MNPs complexes were formed. The samples were subsequently concentrated and separated by magnetic for 10 min to separate the unbound UCNPs−antibody probes. Thereafter, serial dilutions of the supernatants were prepared to examine the fluorescence spectra of the complexes. The 541 nm emission peak excited by a 980 nm laser was used to monitor the AFB_1 concentration (Lu, Chen, Wang, Zheng, & Li, 2015).

As shown in Fig. 6 (A, B, C, D), the fluorescence intensity rapidly decreased as the AFB_1 concentration increased from 0.2 to 100 $ng \cdot mL^{-1}$. A strong linear correlation (R^2 = 0.938) was obtained between various concentrations of AFB_1 (X) and the upconversion luminescent intensity (Fig. 6D). In thinner, secondary, and high three separate concentration phases, linear ratios are all higher than 0.90. It can be seen (Fig. 6) that fluorescence intensity has a minimum linear relationship with lowest concentrations (R^2 =0.904), which is due to the UCNPs nano-particles detection precision; fluorescence intensity has a best linear relationship with high concentrations of AFB_1 (R^2 =0.9822) because of the dense solution and immunization specific recognition precision. The detection limit of this proposed method for AFB_1 was found to be 0.2 $ng \cdot mL^{-1}$. The precision expressed as the relative standard deviation (RSD) of this detection is 3.56% (obtained from a series of 10 standard samples each containing 0.4 $ng \cdot mL^{-1}$). Fig. 6 also depicts a typical recording output for the detection of AFB_1 with different concentrations. Overall, these results demonstrate that the developed method applied here have a good potential to be used as a rapid screening for the detection of mycotoxin ingrain crops.

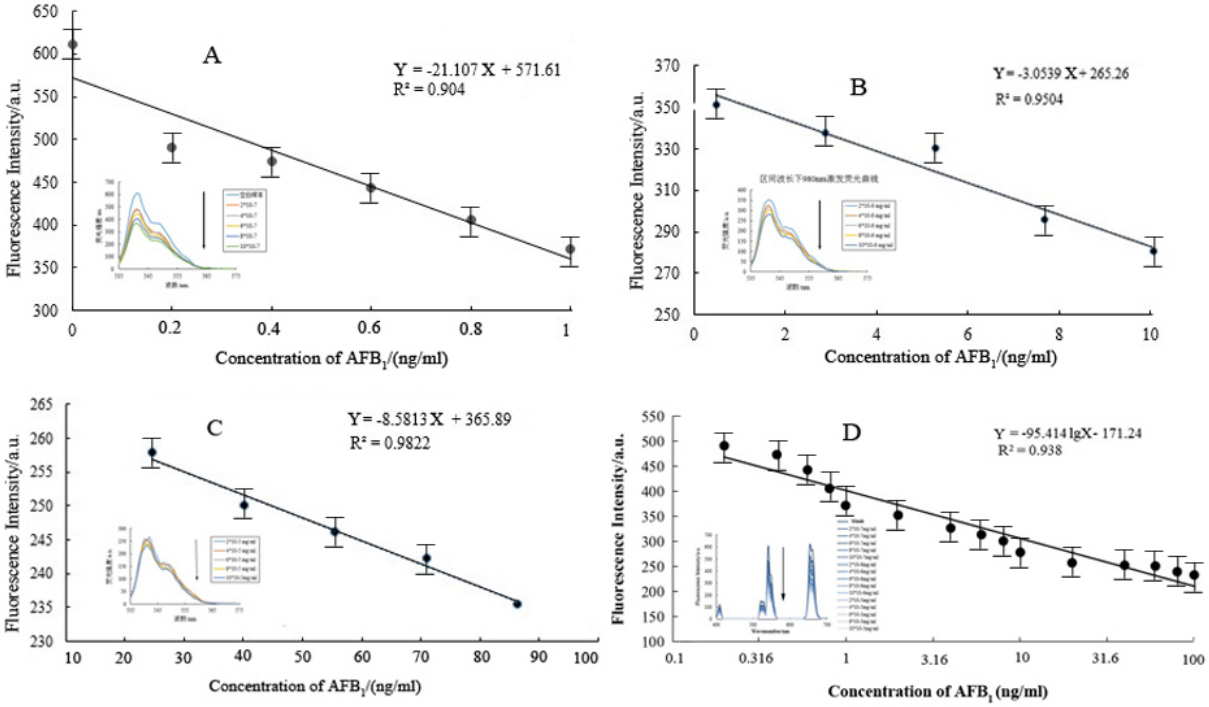

Fig. 6. Linear relation between upconversion luminescent intensity and the various concentrations of AFB_1.

Statistical analysis revealed that the detection limit of AFB_1 are equal to 0.2 $ng \cdot mL^{-1}$, as estimated by using 3σ. These values are desirable for detection AFB_1 in various kinds of foods relative to the maximum acceptable standards of these mycotoxins in China and other countries. The RSD of AFB_1 detection was equal to 3.56% indicating that the developed method exhibited good reproducibility. In the absence of AFB_1-BSA-MNPs, the fluorescence intensity of $NaYF_4$: Yb, Er was at a maximum, and in the presence of AFB_1-BSA-MNPs, the antigen binds with antibody-AFB_1-UCNPs and causes the fluorescent signal of the unreleased UCNPs gradually decreased. It can be understood as that the more MNPs-antigen- antibody-UCNPs was formed, the fewer antibody-UCNPs were remained, and the fluorescence intensity is weaker.

To check feasibility of this method, the accuracy of the measurements of AFB_1 in peanut oil was also evaluated by determining the recovery of AFB_1.by adding a known quantity of standard solution

to the test solution. As shown in Table 1, the recoveries of AFB_1 were between 90.1% and 113.4%, indicating a high level of accuracy of the developed immunoassay. These analyses demonstrated that the proposed method could be applied to the analysis of AFB_1 in real agricultural commodities.

Table 1: Recovery results for AFB_1 detection

Samples	Background concentration（$ng \cdot ml^{-1}$）	Added concentration（$ng \cdot ml^{-1}$）	Detected concentration（$ng \cdot ml^{-1}$)（mean±SD）	Recovery radio%
AFB_1	0.052	0.1	0.150±0.032	98
AFB_1	0.052	1	0.98±0.120	92.8
AFB_1	0.734	0.5	1.301±0.233	113.4
AFB_1	0.734	1	1.720±0.121	98.6
AFB_1	3.364	1	4.265±0.236	90.1
AFB_1	3.364	5	8.465±0.103	102.02

4. Conclusions

In this study, rare earth doped upconversion nanoparticles have been successfully assembled for sensing Aflatoxins B_1 in actual food samples (peanut oil). Herein, antigen-modified magnetic nanoparticles were used for immunosensing probes, and antibody functionalized $NaYF_4$ upconversion nanoparticles as color signal probes. Due to strong fluorescence signal, low autofluorescence of the UCNPs, rapid separation and purification of the magnetic nanoparticles and the immunocomplex, this method can reduce significantly the overall assay time. Based on these results, the ease of use and reliability, the developed method could be extended for the rapid detection of other toxins in the edible oils and other agricultural products. suggest that it maybe be extended to other agriculture products

Acknowledgments

This work has been financially supported by the National Natural Science Foundation of China (31471646) and a Project Funded by the Priority Academic Program Development of Jiangsu Higher Education Institutions (PAPD).

Conflict of interest

The authors declare no conflicts of interest. The authors alone are responsible for the content of this manuscript.

References

Ahn, K.S., Lim, K. R., Jeong, D., Lee, B. Y., Kim, K. S., & Lee, W.Y. (2016). Fluorescence energy transfer inhibition bioassay for cholera toxin based on galactose-stabilized gold nanoparticles and amine-terminated quantum dots. *Microchemical Journal, 124*, 9-14.

Aramburu, I., Galban, J., Ostra, M., Ubide, C., Vidal, M., & Zuriarrain, J. (2015). Uncertainty in CCD detectors with and without cooling devices when used for molecular fluorescence measurements. *Analytical Methods, 7*(6), 2379-2385.

Boyer, J.C., Manseau, M.P., Murray, J. I., & van Veggel, F. C. J. M. (2010). Surface Modification of Upconverting NaYF4 Nanoparticles with PEG-Phosphate Ligands for NIR (800 nm) Biolabeling within the Biological Window. *Langmuir, 26*(2), 1157-1164.

Busman, M., Liu, J., Zhong, H., Bobell, J. R., & Maragos, C. M. (2014). Determination of the aflatoxin AFB1 from corn by direct analysis in real time-mass spectrometry (DART-MS). *Food Additives & Contaminants: Part A, 31*(5), 932-939.

Ceker, S., Agar, G., Alpsoy, L., Nardemir, G., & Kizil, H. E. (2014). Antagonistic effects of Satureja hortensis essential oil against AFB, on human lymphocytes in vitro. *Cytology and Genetics, 48*(5), 327-332.

Chatterjee, D. K., Gnanasammandhan, M. K., & Zhang, Y. (2010). Small Upconverting Fluorescent Nanoparticles for Biomedical Applications. *Small, 6*(24), 2781-2795.

Chatterjee, D. K., Rufaihah, A. J., & Zhang, Y. (2008). Upconversion fluorescence imaging of cells and small animals using lanthanide doped nanocrystals. *Biomaterials, 29*(7), 937-943.

Chen, H.Q., Yuan, F., & Wang, L. (2013). Simple and sensitive turn-on luminescent detection of biothiols based on energy transfer between green-emitting upconversion nanocrystals and gold nanoparticles. *Analytical Methods, 5*(11), 2873-2879.

Chen, K., Fang, J., Peng, X., Cui, H., Chen, J., Wang, F.,Zhou, Y. (2014). Effect of selenium supplementation on aflatoxin B1-induced histopathological lesions and apoptosis in bursa of Fabricius in broilers. *Food and Chemical Toxicology, 74*, 91-97.

Fang, S., Wang, C., Xiang, J., Cheng, L., Song, X., Xu, L.,Liu, Z. (2014). Aptamer-conjugated upconversion nanoprobes assisted by magnetic separation for effective isolation and sensitive detection of circulating tumor cells. *Nano Research, 7*(9), 1327-1336.

Gao, J., Gu, H., & Xu, B. (2009). Multifunctional Magnetic Nanoparticles: Design, Synthesis, and Biomedical Applications. *Accounts of Chemical Research, 42*(8), 1097-1107.

Herzallah, S. M. (2009). Determination of aflatoxins in eggs, milk, meat and meat products using HPLC fluorescent and UV detectors. *Food Chemistry, 114*(3), 1141-1146.

Huang, L.J., Yu, R.Q., & Chu, X. (2015). DNA-functionalized upconversion nanoparticles as biosensors for rapid, sensitive, and selective detection of Hg^{2+} in complex matrices. *Analyst, 140*(15), 4987-4990.

Karimi, M., Habibi-Rezaei, M., Safari, M., Moosavi-Movahedi, A. A., Sayyah, M., Sadeghi, R., & Kokini, J. (2014). Immobilization of endo-inulinase on poly-d-lysine coated $CaCO_3$ micro-particles. *Food Research International, 66*, 485-492.

Klu, Y. A. K., & Chen, J. (2015). Effect of peanut butter matrices on the fate of probiotics during simulated gastrointestinal passage. *LWT - Food Science and Technology, 62*(2), 983-988.

Kozlov, I. A., Melnyk, P. C., Stromsborg, K. E., Chee, M. S., Barker, D. L., & Zhao, C. (2004). Efficient strategies for the conjugation of oligonucleotides to antibodies enabling highly sensitive protein detection. *Biopolymers, 73*(5), 621-630.

Lu, Z., Chen, X., Wang, Y., Zheng, X., & Li, C. (2015). Aptamer based fluorescence recovery assay for aflatoxin B_1

using a quencher system composed of quantum dots and graphene oxide. *Microchimica Acta, 182*(3-4), 571-578.

Luongo, D., Russo, R., Balestrieri, A., Marzocco, S., Bergamo, P., & Severino, L. (2013). In vitro study of AFB_1 and AFM_1 effects on human lymphoblastoid Jurkat T-cell model. *Journal of immunotoxicology, 11*(4), 353-358.

Ma, Y., Liu, H., Han, Z., Yang, L., & Liu, J. (2015). Highly-reproducible Raman scattering of $NaYF_4$:Yb,Er@SiO_2@Ag for methylamphetamine detection under near-infrared laser excitation. *Analyst, 140*(15), 5268-5275.

Maragos, C. (2009). Fluorescence polarization immunoassay of mycotoxins: a review. *Toxins, 1*(2), 196-207.

Mnoyan, A. N., Kirakosyan, A. G., Kim, H., Jang, H. S., & Jeon, D. Y. (2015). Electrostatic Stabilized InP Colloidal Quantum Dots with High Photoluminescence Efficiency. *Langmuir, 31*(25), 7117-7121.

Ong, L. C., Ang, L. Y., Alonso, S., & Zhang, Y. (2014). Bacterial imaging with photostable upconversion fluorescent nanoparticles. *Biomaterials, 35*(9), 2987-2998.

Passone, M. A., Girardi, N. S., & Etcheverry, M. (2013). Antifungal and antiaflatoxigenic activity by vapor contact of three essential oils, and effects of environmental factors on their efficacy. *LWT - Food Science and Technology, 53*(2), 434-444.

Quiles, J. M., Manyes, L., Luciano, F., Mañes, J., & Meca, G. (2015). Influence of the antimicrobial compound allyl isothiocyanate against the Aspergillus parasiticus growth and its aflatoxins production in pizza crust. *Food and Chemical Toxicology, 83*, 222-228.

Sai, N., Chen, Y., Liu, N., Yu, G., Su, P., Feng, Y., Gao, Z. (2010). A sensitive immunoassay based on direct hapten coated format and biotin–streptavidin system for the detection of chloramphenicol. *Talanta, 82*(4), 1113-1121.

Sanders Iii, C. T., DeMasie, C. L., Kerr, W. L., Hargrove, J. L., Pegg, R. B., & Swanson, R. B. (2014). Peanut skins-fortified peanut butters: Effects on consumer acceptability and quality characteristics. *LWT - Food Science and Technology, 59*(1), 222-228.

Sharma, A., Rawat, K., Solanki, P. R., & Bohidar, H. B. (2015). Electrochemical response of agar ionogels towards glucose detection. *Analytical Methods, 7*(14), 5876-5885.

Sozer, N., & Kokini, J. L. (2014). Use of quantum nanodot crystals as imaging probes for cereal proteins. *Food Research International, 57*, 142-151.

Tian, J., Bai, J., Peng, Y., Qie, Z., Zhao, Y., Ning, B.,Gao, Z. (2015). A core-shell-structured molecularly imprinted polymer on upconverting nanoparticles for selective and sensitive fluorescence sensing of sulfamethazine. *Analyst, 140*(15), 5301-5307.

Van de Perre, E., Jacxsens, L., Lachat, C., El Tahan, F., & De Meulenaer, B. (2015). Impact of maximum levels in European legislation on exposure of mycotoxins in dried products: Case of aflatoxin B1 and ochratoxin A in nuts and dried fruits. *Food and Chemical Toxicology, 75*, 112-117.

Waliyar, F., Reddy, S., & Lava-Kumar, P. (2009). Review of immunological methods for the quantification of aflatoxins in peanut and other foods. *Journal Information, 36*(1), 54-59.

Wang, F., Deng, R., Wang, J., Wang, Q., Han, Y., Zhu, H., Liu, X. (2011). Tuning upconversion through energy migration in core–shell nanoparticles. *Nat Mater, 10*(12), 968-973.

Wang, F., Han, Y., Lim, C. S., Lu, Y. H., Wang, J., Xu, J., Liu, X. G. (2010). Simultaneous phase and size control of upconversion nanocrystals through lanthanide doping. *Nature, 463*(7284), 1061-1065.

Wang, L., Li, P., & Li, Y. (2007). Down- and Up-Conversion Luminescent Nanorods. *Advanced Materials, 19*(20), 3304-3307.

Wang, L., & Li, Y. (2006). $Na(Y_{1.5}Na_{0.5})F6$ Single-Crystal Nanorods as Multicolor Luminescent Materials. *Nano Letters, 6*(8), 1645-1649.

Wang, Z., Yue, T., Yuan, Y., Cai, R., Niu, C., & Guo, C. (2013). Preparation of immunomagnetic nanoparticles for the separation and enrichment of Alicyclobacillus spp. in apple juice. *Food Research International, 54*(1), 302-310.

Xia, Q., Huang, X.Y., Xue, F., Zhang, J.J., Zhai, B., Kong, D.C., Long, X.D. (2013). Genetic polymorphisms of DNA repair genes and DNA repair capacity related to aflatoxin b_1 (AFB_1)-induced DNA damages. *New Research Directions in DNA Repair, 1*, 377-412.

Xu, X., Liu, X., Li, Y., & Ying, Y. (2013). A simple and rapid optical biosensor for detection of aflatoxin B_1 based on competitive dispersion of gold nanorods. *Biosensors and Bioelectronics, 47*(0), 361-367.

Yang, B.c., Wang, F., Deng, W., Zou, Y., Liu, F.y., Wan, X.d., Huang, O.p. (2015). Wooden-tip electrospray ionization mass spectrometry for trace analysis of toxic and hazardous compounds in food samples. *Analytical Methods, 7*(14), 5886-5890.

Zhang, Y., Wu, L., Tang, Y., Su, Y., & Lv, Y. (2014). An upconversion fluorescence based turn-on probe for detecting lead(ii) ions.. *Analytical Methods, 6*(22), 9073-9077.

Zhou, J., Liu, Z., & Li, F. (2012). Upconversion nanophosphors for small-animal imaging. *Chemical Society Reviews, 41*(3), 1323-1349.